

ORBITAL-PHASE-DEPENDENT γ -RAY EMISSIONS FROM THE BLACK WIDOW PULSAR

E. M. H. WU¹, J. TAKATA¹, K. S. CHENG¹, R. H. H. HUANG², C. Y. HUI³, A. K. H. KONG², P. H. T. TAM², AND J. H. K. WU²

¹ Department of Physics, University of Hong Kong, Pokfulam Road, Hong Kong; wmheric@gmail.com, takata@hku.hk, hrrspksc@hkucc.hku.hk

² Institute of Astronomy and Department of Physics, National Tsing Hua University, Hsinchu, Taiwan

³ Department of Astronomy and Space Science, Chungnam National University, Daejeon, Korea

Received 2012 August 4; accepted 2012 October 26; published 2012 December 6

ABSTRACT

We report on evidence for orbital phase dependence of the γ -ray emission from the PSR B1957+20 black widow system using data from the *Fermi* Large Area Telescope. We divide an orbital cycle into two regions: one containing the inferior conjunction and the other containing the rest of the orbital cycle. We show that the observed spectra for the different orbital regions are fitted by different functional forms. The spectrum of the orbital region containing the inferior conjunction can be described by a power law with an exponential cutoff (PLE) model, which also gives the best-fit model for the orbital phase without the inferior conjunction, plus an extra component above ~ 2.7 GeV. The emission above 3 GeV in this region is detected with a $\sim 7\sigma$ confidence level. The γ -ray data above ~ 2.7 GeV are observed to be modulated at the orbital period at the $\sim 2.3\sigma$ level. We anticipate that the PLE component dominant below ~ 2.7 GeV originates from the pulsar magnetosphere. We also show that inverse Compton scattering of the thermal radiation of the companion star off a “cold” ultrarelativistic pulsar wind can explain the extra component above ~ 2.7 GeV. The black widow pulsar PSR B1957+20 may be a member of a new class of object, in the sense that the system is showing γ -ray emission with both magnetospheric and pulsar wind origins.

Key words: binaries: close – pulsars: individual (PSR B1957+20) – stars: magnetic fields – stars: neutron

Online-only material: color figures

1. INTRODUCTION

The *Fermi* Large Area Telescope (*Fermi*-LAT) has measured the pulsed γ -ray emission from millisecond pulsars (MSPs), which is magnetospheric in origin (Abdo et al. 2009a, 2009b; Guillemot et al. 2012a). More MSPs have been discovered as *Fermi* unidentified sources in radio bands (e.g., Cognard et al. 2011; Ransom et al. 2011; Guillemot et al. 2012a; Kerr et al. 2012; Ray et al. 2012), suggesting MSPs are some of the major Galactic sources in the high-energy γ -ray sky. Pulsed γ -ray emissions from the energetic MSP, PSR B1957+20, were reported by Guillemot et al. (2012b). PSR B1957+20 is known as the first “black widow” binary system, in which the MSP is destroying its low-mass companion star ($< 0.1 M_{\odot}$) (Fruchter et al. 1988). So far, at least 10 black widow systems have been discovered among the *Fermi* unidentified sources (Roberts 2011; Ray et al. 2012).

Stappers et al. (2003) detected unresolved X-ray emission around PSR B1957+20, and Huang et al. (2012) found the modulation of these unresolved X-ray emissions with orbital period $P_o \sim 9.2$ hr, suggesting the origin of an intra-binary shock (Harding & Gaisser 1990; Arons & Tavani 1993; Cheng et al. 2006). In the intra-binary shock scenario, the wind from the extremely low mass companion is injected by the irradiation of the strong wind/radiation from the MSP and collides with the pulsar wind at a position not far from the companion (Cheng 1989). Pulsed radio emissions from PSR B1957+20 show the eclipse lasting for about 10% of the orbital phase (Fruchter et al. 1988). The corresponding size of the eclipse is on the order of $\sim 10^{11}$ cm, which is larger than the Roche lobe size $\sim 2 \times 10^{10}$ cm, which implies that stellar material is expelled from the companion by the pulsar wind (Ruderman et al. 1989). The irradiation of the pulsar wind/radiation on the companion star of the PSR B1957+20 system was also expected from

observations of the orbital modulation of the optical emissions from the companion (Callanan et al. 1995; Reynolds et al. 2007). In addition to the PSR B1957+20 system, the orbital modulation of the optical emission associated with irradiation of the MSP has been confirmed for several binary systems, for example, the J1023+0038 system (Thorstensen & Armstrong 2005), the black widow system candidates 2FGL J2339.6–0532 (Romani & Shaw 2011; Kong et al. 2012a) and 2FGL J1311.7–3429 (Kataoka et al. 2012; Romani 2012), and accreting MSPs in the quiescent state, e.g., SAX J1808.4–3658 (Burderi et al. 2003; Deloye et al. 2008).

The high-energy emission associated with an intra-binary shock between a pulsar and its companion star was detected from the so-called γ -ray binary PSR B1259-63/LS 2883 system, which is composed of a canonical pulsar with a period $P \sim 48$ ms, and a high-mass Be star (Johnston et al. 1992; Aharonian et al. 2009; Uchiyama et al. 2009). In the γ -ray binary, it has been proposed that the shock stands at the interface between the pulsar wind and the Be wind/disk, and un-pulsed radio to TeV radiation is produced via synchrotron and inverse Compton processes of the accelerated particles at the shock (Tavani & Arons 1997; Dubus 2006; Takata & Taam 2009; Kong et al. 2011, 2012b; Takata et al. 2012). Flare-like GeV emissions were detected by *Fermi* during the 2010/2011 periastron passage (Abdo et al. 2011; Tam et al. 2011). Different models have been proposed to explain the flare-like GeV emission from the PSR B1259–63/LS 2883 system: the Doppler boosting model (Kong et al. 2012b) assumes that the flow in the bow shock tail is relativistic and the synchrotron emission is Doppler boosted, while the pulsar wind model (Khangulyan et al. 2012) assumes that the GeV emissions are produced by the inverse Compton process of the cold relativistic pulsar wind.

The γ -ray emissions associated with the pulsar wind in the black widow system PSR B1957+20 have not yet been

reported. However, we note that for a typical γ -ray binary system, the distance to the shock from the pulsar is of the order of $R_s \sim 0.1\text{--}1$ AU, corresponding to $R_s/R_{lc} \sim 10^4\text{--}10^5$, where $R_{lc} = 2.4 \times 10^8 (P/0.05 \text{ s}) \text{ cm}$ is the light cylinder radius and P is the spin period of the pulsar. For the black widow system, the shock stands at $R_s \sim 10^{10}\text{--}10^{11}$ cm, corresponding to $R_s/R_{lc} \sim 10^3\text{--}10^4$, which is roughly one order of magnitude smaller than that of the γ -ray binaries. Therefore, the black widow system will provide us with a unique laboratory to probe the physics of the pulsar wind and may be a candidate for γ -ray emissions from the pulsar wind. In this paper, we report on the search for orbital modulation of GeV γ -rays from the PSR B1957+20 system from the *Fermi* data to obtain evidence of γ -ray emissions from the intra-binary space.

2. DATA ANALYSIS AND RESULTS

In this analysis, *Fermi*-LAT data were taken between 2008 August 4 and 2011 December 5. We restricted the events in the “source” class (i.e., event class 2) within the “P7SOURCE_V6” instrumental response functions. In addition, we excluded the events with zenith angles greater than 100° to reduce contamination by Earth albedo gamma rays. The data were analyzed using the *Fermi* Science Tools v9r23p1, available from the Fermi Science Support Center.⁴ Events were selected within a circular region of interest (ROI) centered at R.A. = $19^{\text{h}}59^{\text{m}}36^{\text{s}}.77$, decl. = $20^\circ48'15''.1$ (Arzoumanian et al. 1994). In order to reduce systematic uncertainties due to the surrounding complex Galactic region and to achieve better background modeling, photon energies were restricted to be above 200 MeV, and a radius of 5° of the ROI was adopted throughout the analysis. As an attempt to search for evidence of orbital modulation, an orbital phase was assigned to each γ -ray photon based on the timing ephemeris reported by Guillemot et al. (2012b), using the *Fermi* plug-in for TEMPO2,⁵ taking an aperture radius of 1° . No significant evidence of orbital modulation at a $>2\sigma$ level was found by employing the *H*-test (de Jager & Büsching 2010), which is consistent with the results from Guillemot et al. (2012b). To access the effect of the sky exposure as a function of time throughout the observation, a light curve was created with a bin size equal to one-tenth of the orbital period of the binary system, and the exposure was calculated with the tool *gtexposure*. The summed exposure in each bin was found to deviate from the mean value by less than 2%, suggesting that the variation in exposure has a minute effect on the orbital light curve. To avoid bias due to the alignment of the first bin with orbital phase zero, the bins were shifted by phases of 0.2, 0.4, 0.6, and 0.8. The results after shifting the light curve do not alter our conclusion.

Recently, Huang et al. (2012) discovered orbital-modulated X-ray emission from the PSR B1957+20 system. To investigate whether the γ -ray spectral properties also vary with the orbital phase (ϕ), we divided an orbital cycle into two parts: half of the orbit centered at the superior conjunction (hereafter “Phase 1”) and the other half containing the inferior conjunction (hereafter “Phase 2”). Unbinned likelihood analysis was performed for both regions with the help of *glike*. A spectral-spatial model containing all other sources reported in the Second *Fermi* Source Catalog (2FGL hereafter; Nolan et al. 2012) within 10° from the center of the ROI was used for source modeling, resulting in a total of 13 point sources in the model. All the 2FGL sources were assumed to have spectral type as suggested in the catalog.

The spectral parameters of all sources within the ROI were set to be free, while the parameters for sources outside the region were kept fixed. We also included the Galactic diffuse model (*gal_2yearp7v6_v0.fits*) as well as the isotropic spectral template (*iso_p7v6source.txt*) and allowed their normalizations to be free. Since the γ -ray spectra of pulsars in general can be characterized by a power law with an exponential cutoff (PLE) model, $dN/dE = N_0(E/0.2 \text{ GeV})^{-\Gamma} \exp[-(E/E_c)]$ (Abdo et al. 2010), where N_0 is a normalization factor, Γ is the photon index, and E_c is the cutoff energy, we performed a fitting of the spectrum average over each orbit segment with a PLE model. For Phase 1, the best-fit parameters are a photon index of $\Gamma_1 = 0.83 \pm 0.56$ and a cutoff energy of $E_{\text{cutoff},1} = 0.84 \pm 0.30$ GeV, while for Phase 2, $\Gamma_2 = 1.58 \pm 0.30$ and $E_{\text{cutoff},2} = 2.28 \pm 0.88$ GeV. A summary of the fitting results is presented in Table 1. The difference in cutoff energies in the two phases suggests that the spectrum of Phase 2 extends to higher energies than that of Phase 1. Moreover, the observed spectrum of Phase 1 is fitted by the PLE model with a test-statistic (TS) value of 205, while it is fitted by a PL model with a TS value of 168. This indicates that the PLE model is favored over the PL model in describing the spectrum of Phase 1 at a $\sim 6.1\sigma$ confidence level. For Phase 2, the TS values of the best-fit PLE and PL models are 161 and 143, respectively, indicating that the PLE model is not significantly favored over the PL model. The spectral energy distributions for both orbital phases are presented in Figure 1. We computed the extrapolated fluxes in the energy range 0.1–300 GeV for both Phase 1 and Phase 2, which are also presented in Table 1. The values of the fluxes are consistent with those reported in Guillemot et al. (2012b) within uncertainties. We note that in the source model, the best-fit log-parabola model for the source 2FGL J1949.7+2405 yields a curvature coefficient $\beta \approx 0.2\text{--}0.3$, which is different from that given in the 2FGL catalog, where the value of β is fixed at 1. However, it is pointed out in Nolan et al. (2012) that such a highly curved spectrum is not necessarily robust, possibly due to the densely populated region near the Galactic plane. Moreover, a likelihood analysis using an ROI of radius 15 deg (see below) yields a similar result, suggesting that the deviation could be justifiable.

Since the radius of the point-spread function (PSF) is relatively large near the low-energy bound of 200 MeV, the spectral results may be affected by the wings of the PSFs of surrounding sources. Thus, we performed a binned likelihood analysis with an ROI of radius 15° around PSR B1957+20. The spectral fitting results are presented in Table 1. These results are consistent with those obtained using an ROI of radius 5° . We also note that the difference in the best-fit cutoff energies in Phase 1 and Phase 2 agrees with the conclusion on the difference in the spectral properties of the two orbital phases.

By comparing the γ -ray spectra, we speculate that the spectrum for Phase 2 can be described by two components, one magnetospheric, which has also been well established by Guillemot et al. (2012b), and the other above ~ 3 GeV, coming from the interaction between the pulsar wind and the companion star. To describe this component while avoiding bias toward any emission scenario, we adopted a simple Gaussian profile $dN/dE = A \exp[-(E - \bar{E})^2/\sigma_G^2]$ to fit the data along with a PLE model with the spectral index and the cutoff energy fixed at the best-fit values derived from Phase 1. The best-fit two-component model is presented as the solid line in the right panel of Figure 1. The best-fit parameters for the Gaussian component are $\bar{E} = 3.76 \pm 0.59$ GeV and $\sigma_G = 1.10 \pm 0.39$ GeV. To

⁴ <http://fermi.gsfc.nasa.gov/ssc/data/analysis/software/>

⁵ See http://fermi.gsfc.nasa.gov/ssc/data/analysis/user/Fermi_plug_doc.pdf

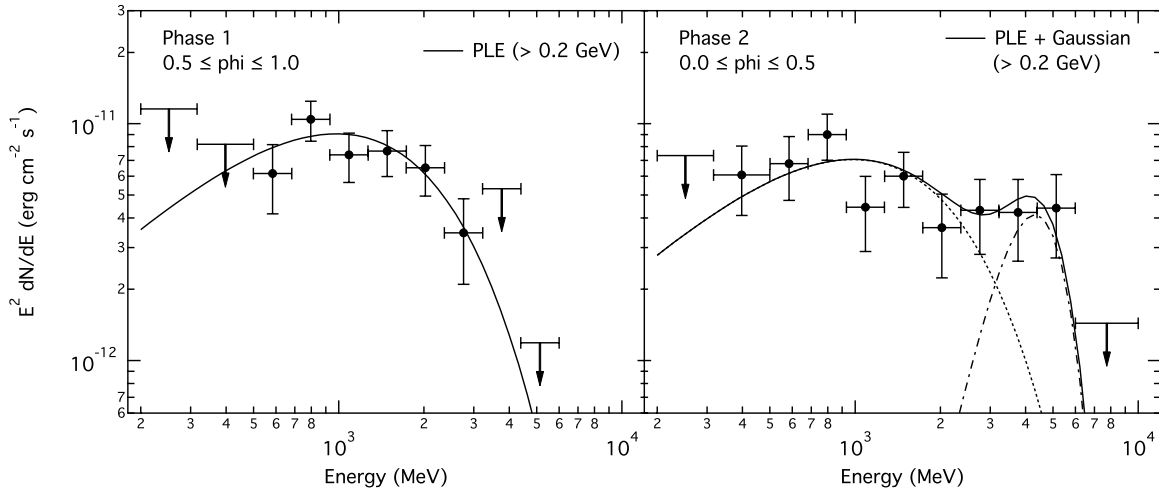


Figure 1. Spectral energy distributions of γ -ray emission from PSR B1957+20. Data points were derived from likelihood fitting of individual energy bins, in which a simple power law (PL) is used to model the data. 90% upper limits were calculated for any energy bin in which the detection significance is lower than 3σ . Left: spectrum averaged over Phase 1. The solid line shows the best-fit PLE model from fitting the data above 0.2 GeV. Right: spectrum averaged over Phase 2. The solid line represents the fitted two-component model, with the PLE component shown as a dashed line and the Gaussian component shown as a dash-dotted line.

Table 1
Summary of Spectral Fitting Results of the Two Orbital Phases

Orbital Phase	ROI Radius ($^{\circ}$) (Analysis Type)	Spectral Model	Γ	E_c (GeV)	\bar{E} (GeV)	σ_G (GeV)	Flux ^a (10^{-9} photon cm^{-2} s^{-1})
0.5–1.0 (Phase 1)	5 (unbinned)	PLE	0.83 ± 0.56	0.84 ± 0.30	8.95 ± 1.79 (12.8 ± 4.42)
	15 (binned)	PLE	1.21 ± 0.57	1.04 ± 0.46	8.76 ± 1.99 (14.3 ± 5.94)
0.0–0.5 (Phase 2)	5 (unbinned)	PLE	1.58 ± 0.30	2.28 ± 0.88	8.47 ± 1.57 (15.0 ± 4.52)
	5 (unbinned)	PLE + Gaussian	0.83^b	0.84^b	3.76 ± 0.59	1.10 ± 0.39	7.19 ± 0.85 (10.2 ± 1.22)
	15 (binned)	PLE	1.88 ± 0.19	3.17 ± 1.15	8.12 ± 1.28 (16.6 ± 3.77)
	15 (binned)	PLE + Gaussian	1.21^b	1.04^b	3.80 ± 0.70	1.00 ± 0.54	6.76 ± 0.96 (10.9 ± 1.57)

Notes.

^a Integrated photon flux in the energy range 0.2–300 GeV. The values in brackets represent the 0.1–300 GeV extrapolated photon flux.

^b Model parameters without quoted errors are fixed at the values given.

access the significance of the emission of this extra component, we performed a likelihood analysis using the data at energies above $\bar{E} - \sigma_G \approx 2.7$ GeV by assuming a simple PL model, alleviating the effect of the spectral model on the significance. For Phase 2, a TS value of 55 was achieved, corresponding to a significance of $\sim 7\sigma$, whereas for Phase 1, a TS value of 14 was obtained, indicating that the detection significance is below 4σ at >2.7 GeV for Phase 1. We computed the TS maps using *gttstmap* at energies >2.7 GeV for both Phase 1 and Phase 2, which are shown in Figure 2(a). The difference in the TS values for the two orbital phases is readily observable by comparing the maps.

In addition, we investigate the relation between the rotation phase of the pulsar and the variation of spectral characteristics in the two orbital phases by removing the pulsed component. A pulse profile of PSR B1957+20 was constructed by phase folding the photons with energies above 0.2 GeV and within an angular distance of 1° from the position of the pulsar. The gamma-ray peaks in the profile were then fitted with two Lorentzian functions. Data were removed from within the full widths at half-maximum of the fitted peaks which consist of phases 0.103–0.215 and 0.598–0.620. The pulse profile and

the fitted Lorentzian functions are illustrated in Figure 3. We compare the significance of the emission in Phase 2 below and above 2.7 GeV, before and after removing the pulsation peaks. At energies below 2.7 GeV, the TS value decreased from 105 to 38, while at energies above 2.7 GeV, the TS value decreased from 55 to 36. Figures 2(b) and (c) show the TS maps for a visual comparison before and after the removal of the pulsed component.

The above results indicate the presence of emission above 2.7 GeV, which is clearly detected in Phase 2 but not in Phase 1. Hence, the γ -ray emission from PSR B1957+20 is dependent on the orbital phase of the binary system. Moreover, the removal of the pulsed emission component has caused a greater decrease in the detection significance at energies below 2.7 GeV than above, implying that the majority of the emission at 2.7 GeV in Phase 2 is not produced inside the pulsar magnetosphere, but in the intra-binary region.

Since the best-fit two-component model suggests that photons at $\gtrsim 2.7$ GeV may be modulated with the orbital phase, we constructed a phase-folded light curve and derived the significance of the modulation. To allow for enough photon statistics, we selected events with energies greater than 2.7 GeV, the size

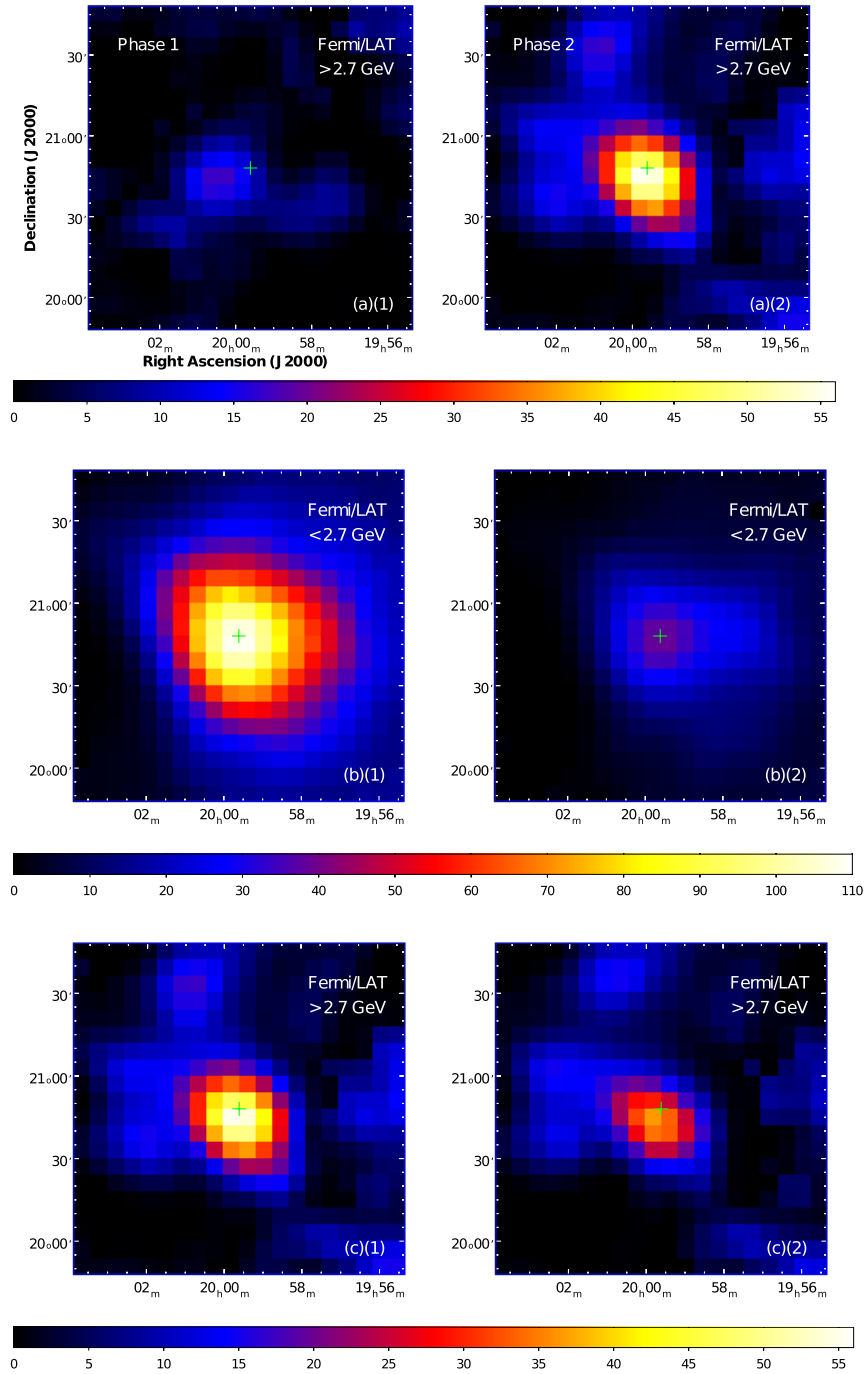


Figure 2. Test-statistic (TS) maps of $2^\circ \times 2^\circ$ regions centered at the position of PSR B1957+20 (labeled by green crosses). The color scale below each pair of images is used to indicate the TS values. (a): (1) TS map at energy >2.7 GeV using only photons in Phase 1. (2) Same as (a)(1) but using only photons in Phase 2. (b): (1) TS map at <2.7 GeV for Phase 2. (2) Same as (b)(1) but with data within full width at half-maximum of the pulsation peaks removed (see the text). (c): Same as (b) but with energy >2.7 GeV. (A color version of this figure is available in the online journal.)

r of the aperture. The best profile ($r = 0.965$) is presented in Figure 4, with an H -test TS of 19 (de Jager & Büsching 2010), corresponding to a significance of $\sim 3.3\sigma$. The post-trial significance, associated with 21 trials on the aperture radius, is $\sim 2.3\sigma$.

3. DISCUSSION

We have reported the evidence of orbital-modulated GeV γ -ray emission from the black widow system PSR B1957+20. We have fitted the spectrum of Phase 2 (half of the orbit centered

at the inferior conjunction) using the best-fit PLE model of Phase 1 plus the Gaussian component with $\bar{E} = 3.76 \pm 0.59$ GeV and $\sigma_G = 1.10 \pm 0.39$ GeV. The additional component in the spectrum has been found with a $\sim 7\sigma$ confidence level. We have also shown that the orbital modulation above ~ 3 GeV can be found with a $\sim 2.3\sigma$ confidence level.

It can be expected that the PLE component below 3 GeV will be dominated by the emission from the pulsar magnetosphere. For the additional component above 3 GeV in Phase 2, we will speculate on the possibility of the inverse Compton process of

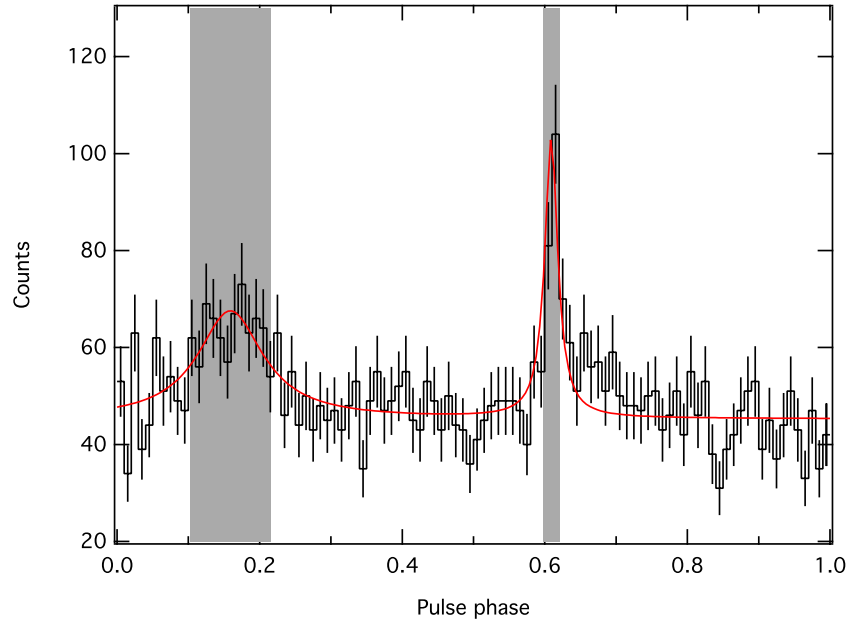


Figure 3. Pulse profile of the γ -ray emission from PSR B1957+20, produced using data above 0.2 GeV and within 1° from the position of the pulsar. The red solid line represents the fitted Lorentzian functions. The shaded regions indicate the pulse phases within the full widths at half-maximum of the two peaks.

(A color version of this figure is available in the online journal.)

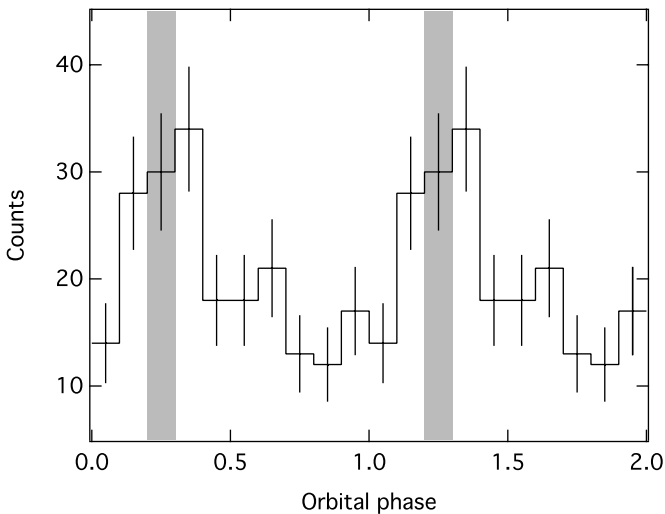


Figure 4. γ -ray light curve of PSR B1957+20 folded at the orbital period using the *Fermi* plug-in for TEMPO2, with the optimized size of aperture of 0.965 . Two orbits are shown for clarity. The shaded regions correspond to the phase of the radio eclipse, which is the center of Phase 2.

a “cold” ultrarelativistic pulsar wind. In this section, we will calculate the expected spectra of the emissions from the pulsar magnetosphere and from the pulsar wind.

3.1. Outer Gap Emissions

For the magnetospheric emission, we apply the two-layer outer gap model explored by Wang et al. (2010, 2011). The dashed lines in Figure 5 represent the calculated phase-averaged spectra of the curvature radiation from the outer gap. The results are for an inclination angle of $\alpha = 60^\circ$ and a viewing angle of $\xi = 80^\circ$, which were assumed to explain the pulse profile and the spectrum. A larger viewing angle is required to explain the phase separation (~ 0.45 orbital phase) of the two peaks in the light curve of the pulsed emissions. The assumed

viewing geometry is consistent with that used in Guillemot et al. (2012b). For the present outer gap model, the γ -ray luminosity is expected to be of the order of $L_{\text{gap}} \sim f^3 L_{\text{sd}}$, where f is the fractional gap thickness, which is the ratio of the gap thickness to the light cylinder radius at the light cylinder, and $L_{\text{sd}} \sim 1.6 \times 10^{35} \text{ erg s}^{-1}$ (Manchester et al. 2005)⁶ is the spin-down power of PSR B1957+20. We note that because the period time derivatives before and after correction for the Shklovskii effect (Shklovskii 1970) due to proper motion are $\dot{P} \sim 1.68 \times 10^{-20}$ and $\sim 1.13 \times 10^{-20}$ (Manchester et al. 2005), respectively, the spin-down power and hence our main conclusion are not greatly changed by the Shklovskii effect. For the fractional gap thickness, we apply the outer gap model controlled by the magnetic pair-creation process near the stellar surface (Takata et al. 2010), which implies $f \sim 2.5(P/0.1 \text{ s})^{1/2} \sim 0.3$ for PSR B1957+20. The right panel in Figure 5 compares the model spectrum of the outer gap and the observed γ -ray spectrum in the off-peak orbital phase in Figure 4, where we expect that the magnetospheric emission dominates. We can see in Figure 5 that the emissions from the outer gap can well explain the *Fermi* data in the off-peak orbital phase.

3.2. Pulsar Wind Emissions

It is thought that a “cold” pulsar wind, which is mainly composed of electrons and positron pairs, is injected into the interstellar space by the pulsars. The pulsar wind is accelerated beyond the light cylinder to a Lorentz factor $\Gamma_w \sim 10^5$ – 10^7 (Kennel & Coroniti 1984). If the cold ultrarelativistic pulsar wind interacts with the interstellar medium, the kinetic energy of the pulsar wind is converted into internal energy at the shock. The shocked pulsar wind can emit X-rays via synchrotron radiation and is observed as the pulsar wind nebula. The unshocked cold pulsar wind is dark in the X-ray bands, because the wind does not emit synchrotron photons. However, it can be thought that the cold ultrarelativistic pulsar wind emits very high

⁶ <http://www.atnf.csiro.au/research/pulsar/psrcat>

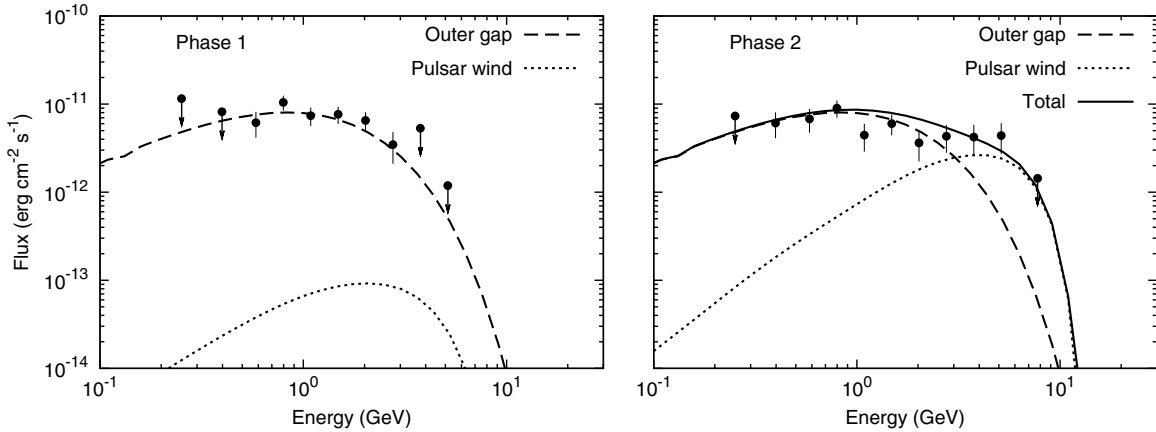


Figure 5. Spectrum averaged over Phase 1 (left panel) and Phase 2 (right panel). The dashed and dotted lines are the spectra of the emissions from the outer gap and the cold ultrarelativistic pulsar wind, respectively. The solid line represents the total contribution from the components.

energy γ -rays by the inverse Compton process between the cold pulsar wind and the background soft photons from the pulsar magnetosphere or from the companion in the binary system. In fact, studies have been carried out on the γ -ray emissions from the cold pulsar wind of the Crab pulsar (Aharonian et al. 2012) and of the γ -ray binary PSR B1259–63 (Khangulyan et al. 2007, 2012; Takata & Taam 2009).

For PSR B1957+20 black widow system, the temperature of the heating side of companion is as high as $T_{\text{eff}} \sim 8300$ K (Reynolds et al. 2007). Roughly speaking, the luminosity of the inverse Compton process may be estimated by $L_{\text{IC}} \sim (1 - \cos \theta_0) \sigma_T n_{\text{ph}} a_s L_{\text{sd}} \sim 5 \times 10^{-3} (1 - \cos \theta_0) (T_{\text{eff},3}/8.3)^3 R_{s,10}^2 a_{s,11}^{-1} L_{\text{sd}}$, where θ_0 is the collision angle between the pulsar wind and the soft photon, $R_s \sim 10^{10} R_{s,10}$ cm is the Roche lobe radius, and $a_s = 10^{11} a_{s,11}$ cm is the separation between the pulsar and the companion. In addition, $n_{\text{ph}} \sim \sigma_{\text{sb}} T_{\text{eff}}^3 R_s^2 / k_B c a_s^2$ with k_B being the Boltzmann constant, is the typical number density of the soft-photon field, and $T_{\text{eff},3} = (T_{\text{eff}}/1000 \text{ K})$. Because the typical luminosity of outer gap emissions is of the order of $L_{\text{gap}} \sim f^3 L_{\text{sd}} \sim 0.03 L_{\text{sd}}$, the inverse Compton process of the pulsar wind may produce γ -ray radiation with a flux level that is of the same order of magnitude as that of the gap emissions, if the inverse Compton process occurs as a head-on collision, which can happen around the inferior conjunction because the companion is located between the pulsar and the Earth. In fact, we have measured the significant excess of the γ -ray emissions above 3 GeV during the inferior conjunction passage. The typical energy of the scattered photons is $\sim 3 \Gamma_w^2 k T_{\text{eff}} \sim 5 \text{ GeV} (T_{\text{eff},3}/8.3) (\Gamma_w/5 \times 10^4)^2$.

We perform a more detail calculation for the inverse Compton process between the cold ultrarelativistic pulsar wind and the soft-photon field from the companion. The emissivity of the inverse Compton process of a particle may be expressed as (Begelman & Sikora 1987; Takata et al. 2012)

$$\frac{dP_{\text{IC}}}{d\Omega} = D^2 \int_0^{\theta_c} (1 - \beta \cos \theta_0) I_b / h \frac{d\sigma'_{\text{KN}}}{d\Omega'} d\Omega_0, \quad (1)$$

where $d\sigma'_{\text{KN}}/d\Omega'$ is the differential Klein–Nishina cross section, $\beta = \sqrt{\Gamma_w^2 - 1}/\Gamma_w$, $D = \Gamma_w^{-1} (1 - \beta \cos \theta_1)^{-1}$ with θ_1 being the angle between the direction of the particle motion and the propagating direction of the scattered photon, h is the Planck constant, I_b is the background photon field, and θ_c expresses the angular size of star as seen from the emission point.

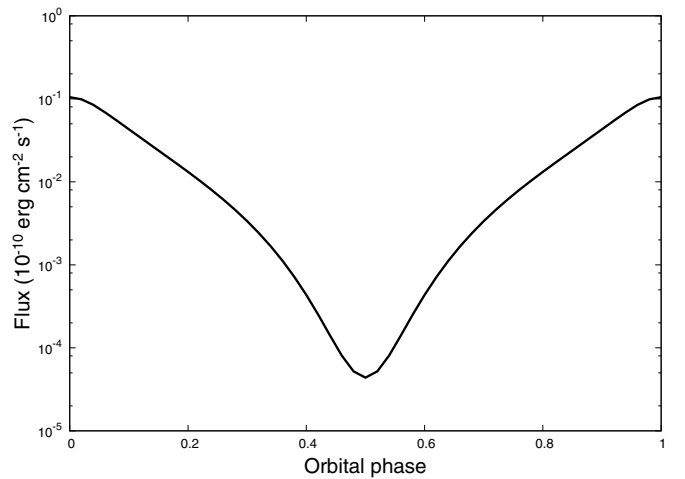


Figure 6. Calculated orbital modulation for γ -ray emissions from the inverse Compton process of a cold ultrarelativistic pulsar wind. The phase zero corresponds to the inferior conjunction.

We assume that all the pulsar wind’s particles have a Lorentz factor of $\Gamma_w = 4 \times 10^4$. We consider that the energy flux of the pulsar wind depends on the colatitude (θ) measured from the rotation axis as $L_w(\theta) \propto \sin^2 \theta$ (Bogovalov & Khangouljan 2002; Lyubarsky 2002), and that the total power of the wind corresponds to the spin-down power. We also assume that half of the energy flux is carried by the kinetic energy of the pulsar wind. The fitting of the optical modulation using the ELC model implies that the inclination angle of the orbital plane with respect to the sky is $i \sim 65^\circ$ (Reynolds et al. 2007). In the present calculation, we assume $i = 67^\circ$ and the viewing angle $\xi = 80^\circ$ with respect to the rotation axis of PSR B1957+20. The distance to the source has been estimated as $d \sim 2.5 \pm 1$ kpc (Fruchter et al. 1988; Guillemot et al. 2012b). In the present calculation, we apply $d = 2$ kpc. We note that the observed flux can be reproduced more easily with a larger inclination angle and a smaller distance than the estimated values within their uncertainties.

The spectra of the inverse Compton process of the pulsar wind are described by the dotted lines in Figure 5, and the temporal behavior is summarized in Figure 6, where the phase zero corresponds to the inferior conjunction. We expect that the pulsar passes the inferior conjunction at the center of the X-ray peak phase (Phase 2). At the inferior conjunction passage,

because the companion is located between the pulsar and the Earth, the inverse Compton process occurs as a head-on collision rather than a tail-on collision. We found that the emission from the inverse Compton process dominates the curvature radiation from the outer gap in the spectrum above 3 GeV and can explain the observed excess in the *Fermi* data at the peak orbital phase, as the left panel in Figure 5 indicates. In the off-peak phase (Phase 1), because the inverse Compton process occurs as a tail-on collision rather than head-on, the inverse Compton process is suppressed. Hence, only magnetospheric emission contributes to the observed emissions, as shown in the right panel of Figure 5.

As we have seen, the inverse Compton process of the cold ultrarelativistic pulsar wind can explain the observed extra component above 3 GeV in the orbital phases around the inferior conjunction. Hence, we would like to emphasize that the PSR B1957+20 binary system is (1) a plausible candidate to manifest the emission from the cold ultrarelativistic wind and (2) a candidate for the new class of γ -ray binary, in the sense that the γ -ray binary is composed of an MSP and a low-mass star, and shows both magnetospheric and pulsar wind emissions.

It is unlikely that the extra component above 3 GeV during the inferior conjunction passage originates from the inverse Compton process of the *shocked* pulsar wind. We may estimate the magnetic field of the pulsar wind after the shock by $B = 3L_{\text{sd}}^{1/2} a_s c^{-1/2} \sigma_w^{1/2} (1 + \sigma_w)^{-1/2}$ (Takata & Taam 2009), where σ_w is the ratio of the magnetic energy to the particle energy at the shock. The energy density of the thermal radiation from the companion is at most $U_{\text{ph}} = \sigma_{\text{SB}} T_{\text{eff}}^4 / c$. Hence, the ratio of powers of the synchrotron radiation and the inverse Compton process of the shocked pulsar wind is estimated as $U_B / U_{\text{ph}} \sim 10L_{\text{sd},35}^{1/2} (T_{\text{eff},3/8.3})^{-4} \sigma_w (1 + \sigma_w)$, where $L_{\text{sd},35} = (L_{\text{sd},35} / 10^{35} \text{ erg s}^{-1})$. On the other hand, the ratio of the observed fluxes of the orbital modulated X-ray emissions ($\sim 10^{-13} \text{ erg cm}^{-2} \text{ s}^{-1}$; Huang et al. 2012) and GeV emissions ($\sim 10^{-11} \text{ erg cm}^{-2} \text{ s}^{-1}$) is $\sim 10^{-2}$. Hence, the inverse Compton process of the shocked pulsar wind will not explain the emissions above ~ 3 GeV observed at the inferior conjunction passage.

Finally, we remark that the black widow pulsars discovered among *Fermi* unidentified sources are good targets for searching for orbital phase-dependent γ -ray spectra. In particular, the black widow candidates 2FGL J2339.6–0532 and 2FGL J1311.7–3429 show orbital modulation in the optical, and it is evident that the former candidate shows X-ray modulation as well. Hence, they are an excellent probe for γ -ray emission with both magnetospheric and pulsar wind components.

In summary, despite the limitation from the significance of each individual approach, the evidence as a whole has allowed us to confirm the detection of orbital modulated γ -rays from the PSR B1957+20 system from *Fermi*-LAT data. We have shown that the significant emissions above 3 GeV appear around inferior conjunction, while the emissions below 3 GeV are steady and are described by the pulsar emissions. We expect that the modulated emissions above 3 GeV originate from the inverse Compton scattering of the thermal radiation of the companion star off the cold ultrarelativistic pulsar wind.

We thank P. Ray for useful discussions and suggestions for *Fermi* data analysis. We express our appreciation to the anonymous referee for useful comments and suggestions. This project is supported by the National Science Council of the Republic

of China (Taiwan) through grants NSC100-2628-M-007-002-MY3, NSC100-2923-M-007-001-MY3, and NSC101-2112-M-007-022-MY3. C.Y.H. is supported by the National Research Foundation of Korea through grant 2011-0023383. A.K.H.K. gratefully acknowledges support from a Kenda Foundation Golden Jade Fellowship. E.M.H.W., J.T., and K.S.C. are supported by a GRF grant of HK Government under HKU700911P.

REFERENCES

- Abdo, A. A., Ackermann, M., Ajello, M., et al. 2009a, *Science*, **325**, 848
 Abdo, A. A., Ackermann, M., Ajello, M., et al. 2010, *ApJS*, **187**, 460
 Abdo, A. A., Ackermann, M., Ajello, M., et al. 2011, *ApJ*, **736**, L11
 Abdo, A. A., Ackermann, M., Atwood, W. B., et al. 2009b, *ApJ*, **699**, 1171
 Aharonian, F., Akhperjanian, A. G., Anton, G., et al. 2009, *A&A*, **507**, 389
 Aharonian, F. A., Bogovalov, S. V., & Khangulyan, D. 2012, *Nature*, **482**, 507
 Arons, J., & Tavani, M. 1993, *ApJ*, **403**, 249
 Arzoumanian, Z., Fruchter, A. S., & Taylor, J. H. 1994, *ApJ*, **426**, L85
 Begelman, M. C., & Sikora, M. 1987, *ApJ*, **322**, 650
 Bogovalov, S. V., & Khangoulian, D. V. 2002, *MNRAS*, **336**, L53
 Burderi, L., Di Salvo, T., D'Antona, F., Robba, N. R., & Testa, V. 2003, *A&A*, **404**, L43
 Callanan, P. J., van Paradijs, J., & Rengelink, R. 1995, *ApJ*, **439**, 928
 Cheng, A. F. 1989, *ApJ*, **339**, 291
 Cheng, K. S., Taam, R. E., & Wang, W. 2006, *ApJ*, **641**, 427
 Cognard, I., Guillemot, L., Johnson, T. J., et al. 2011, *ApJ*, **732**, 47
 de Jager, O. C., & Büsching, I. 2010, *A&A*, **517**, L9
 Deloye, C. J., Heinke, C. O., Taam, R. E., & Jonker, P. G. 2008, *MNRAS*, **391**, 1619
 Dubus, G. 2006, *A&A*, **456**, 801
 Fruchter, A. S., Stinebring, D. R., & Taylor, J. H. 1988, *Nature*, **333**, 237
 Guillemot, L., Freire, P. C. C., Cognard, I., et al. 2012a, *MNRAS*, **422**, 1294
 Guillemot, L., Johnson, T. J., Venter, C., et al. 2012b, *ApJ*, **744**, 33
 Harding, A. K., & Gaissner, T. K. 1990, *ApJ*, **358**, 561
 Huang, R. H. H., Kong, A. K. H., Takata, J., et al. 2012, *ApJ*, **760**, 92
 Johnston, S., Manchester, R. N., Lyne, A. G., et al. 1992, *ApJ*, **387**, L37
 Kataoka, J., Yatsu, Y., Kawai, N., et al. 2012, *ApJ*, **757**, 176
 Kennel, C. F., & Coroniti, F. V. 1984, *ApJ*, **283**, 710
 Kerr, M., Camilo, F., Johnson, T. J., et al. 2012, *ApJ*, **748**, L2
 Khangulyan, D., Aharonian, F. A., Bogovalov, S. V., & Ribó, M. 2012, *ApJ*, **752**, L17
 Khangulyan, D., Hnatic, S., Aharonian, F., & Bogovalov, S. 2007, *MNRAS*, **380**, 320
 Kong, A. K. H., Huang, R. H. H., Cheng, K. S., et al. 2012a, *ApJ*, **747**, L3
 Kong, S. W., Cheng, K. S., & Huang, Y. F. 2012b, *ApJ*, **753**, 127
 Kong, S. W., Yu, Y. W., Huang, Y. F., & Cheng, K. S. 2011, *MNRAS*, **416**, 1067
 Lyubarsky, Y. E. 2002, *MNRAS*, **329**, 34
 Manchester, R. N., Hobbs, G. B., Teoh, A., & Hobbs, M. 2005, *AJ*, **129**, 1993
 Nolan, P. L., Abdo, A. A., Ackermann, M., et al. 2012, *ApJS*, **199**, 31
 Ransom, S. M., Ray, P. S., Camilo, F., et al. 2011, *ApJ*, **727**, L16
 Ray, P. S., Abdo, A. A., Parent, D., et al. 2012, Proc. 2011 Fermi Symp. (arXiv:1205.3089)
 Reynolds, M. T., Callanan, P. J., Fruchter, A. S., et al. 2007, *MNRAS*, **379**, 1117
 Roberts, M. S. E. 2011, in AIP Conf. Proc. 1357, Radio Pulsars: An Astrophysical Key to Unlock the Secrets of the Universe (Melville, NY: AIP), **127** (arXiv:1103.0819)
 Romani, R. W. 2012, *ApJ*, **754**, L25
 Romani, R. W., & Shaw, M. S. 2011, *ApJ*, **743**, L26
 Ruderman, M., Shaham, J., Tavani, M., & Eichler, D. 1989, *ApJ*, **343**, 292
 Shklovskii, I. S. 1970, *SvA*, **13**, 562
 Stappers, B. W., Gaensler, B. M., Kaspi, V. M., van der Klis, M., & Lewin, W. H. G. 2003, *Science*, **299**, 1372
 Takata, J., Okazaki, A. T., Nagataki, S., et al. 2012, *ApJ*, **750**, 70
 Takata, J., & Taam, R. E. 2009, *ApJ*, **702**, 100
 Takata, J., Wang, Y., & Cheng, K. S. 2010, *ApJ*, **715**, 1318
 Tam, P. H. T., Huang, R. H. H., Takata, J., et al. 2011, *ApJ*, **736**, L10
 Tavani, M., & Arons, J. 1997, *ApJ*, **477**, 439
 Thorstensen, J. R., & Armstrong, E. 2005, *AJ*, **130**, 759
 Uchiyama, Y., Tanaka, T., Takahashi, T., Mori, K., & Nakazawa, K. 2009, *ApJ*, **698**, 911
 Wang, Y., Takata, J., & Cheng, K. S. 2010, *ApJ*, **720**, 178
 Wang, Y., Takata, J., & Cheng, K. S. 2011, *MNRAS*, **415**, 1827